

Particle Size Distribution, Concentration, and Magnetic Attraction Affect Transport of Polymer-Modified Fe⁰ Nanoparticles in Sand Columns

TANAPON PHENRAT,[†] HYE-JIN KIM,[†]
FRITJOF FAGERLUND,[‡]
TISSA ILLANGASEKARE,[‡]
ROBERT D. TILTON,^{§,||} AND
GREGORY V. LOWRY^{*,†,§}

Center for Environmental Implications of Nanotechnology (CEINT) and Department of Civil & Environmental Engineering, Department of Chemical Engineering, and Department of Biomedical Engineering, Carnegie Mellon University, Pittsburgh, Pennsylvania 15213-3890, and Center for Experimental Study of Subsurface Environmental Processes at Colorado School of Mines, Golden, Colorado 80401

Received January 18, 2009. Revised manuscript received April 16, 2009. Accepted May 1, 2009.

The effect of particle concentration, size distribution (polydispersity) and magnetic attractive forces (Fe⁰ content) on agglomeration and transport of poly(styrene sulfonate) (PSS) modified NZVI was studied in water-saturated sand ($d_p = 300 \mu\text{m}$) columns. Particle concentrations ranged from 0.03 to 6 g/L in 5 mM NaCl/5 mM NaHCO₃ at a pore water velocity of 3.2×10^{-4} m/s. Three NZVI dispersions with different intrinsic particle size distributions obtained from sequential sedimentation are compared. The influence of magnetic attraction (Fe⁰ content) on NZVI agglomeration and deposition in porous media is assessed by comparing the deposition behavior of PSS-modified NZVI (magnetic) having different Fe⁰ contents with PSS-modified hematite (nonmagnetic) with the same surface modifier. At low particle concentration (30 mg/L) all particles were mobile in sand columns regardless of size or magnetic attractive forces. At high concentration (1 to 6 g/L), deposition of the relatively monodisperse dispersion containing PSS-modified NZVI (hydrodynamic radius (R_H) = 24 nm) with the lowest Fe⁰ content (4 wt %) is low (attachment efficiency (α) = 2.5×10^{-3}), insensitive to particle concentration, and similar to PSS-modified hematite. At 1 to 6 g/L, the attachment efficiency of polydisperse dispersions containing both primary particles and sintered aggregates (R_H from 15 to 260 nm) of PSS-modified NZVI with a range of Fe⁰ content (10–60%) is greater (α = 1.2×10^{-2} to 7.2×10^{-2}) and is sensitive to particle size distribution. The greater attachment for larger, more polydisperse Fe⁰

nanoparticles with higher Fe⁰ content is a result of their agglomeration during transport in porous media because the magnetic attractive force between particles increases with the sixth power of particle/agglomerate radius. A filtration model that considers agglomeration in porous media and subsequent deposition explains the observed transport of polydisperse PSS-modified NZVI at high concentration.

Introduction

In situ groundwater and soil remediation can potentially benefit from nanotechnology. The ability of Fe⁰ nanoparticles (“nanoscale zerovalent iron”, NZVI) to rapidly dechlorinate chlorinated organics (1, 2) or to immobilize heavy metals (3) found in contaminated groundwater is well documented and initial field demonstrations are promising (4). Controlled emplacement of NZVI in the contaminant source zone is essential for the success of *in situ* remediation using NZVI. However, we currently lack the fundamental understanding of the physicochemical and hydrogeochemical factors affecting the emplacement of NZVI, especially at high NZVI particle concentration used for remediation (1 to 10 g/L). This study determines the effects of intrinsic particle size distribution, concentration, and magnetic attraction between particles on NZVI aggregation and its transport in porous media.

Bare NZVI particles rapidly aggregate (5) and readily deposit onto aquifer materials (6), rendering them immobile in the subsurface (6, 7). For this reason, the NZVI particles are embedded in a silica matrix (8) or modified by physisorption of charged macromolecules (polyelectrolytes) (9). The polymeric surface modification provides the particles with electrosteric repulsive forces, i.e. a combination of steric repulsion and electrostatic repulsion (10). The electrosteric interaction between a polyelectrolyte-modified NZVI and a collector (e.g., sand grains) decreases the probability of particle attachment and therefore enhances particle mobility in the subsurface (6, 11–14). The range and magnitude of the electrosteric repulsion between two particles depends on the surface concentration of the adsorbed polyelectrolyte and the extension and charge density of the adsorbed polyelectrolyte layer (10). However, adsorbed polyelectrolyte can only stabilize a fraction of NZVI which is polydisperse (10, 15). The largest NZVI particles present as sintered aggregates are not stabilized by any modifier and rapidly agglomerate to micrometer sized fractal agglomerates, as is also observed for bare NZVI. This nondispersible fraction is attributed to strong magnetic attractions among the larger sintered aggregates present in the polydisperse NZVI slurry, as the magnetic attractive force increases with particle radius to the sixth power (10).

Transport and deposition of NZVI or other reactive nanomaterials in porous media is typically studied at low particle concentration (<30 mg/L) and modeled using deep-bed filtration models (11, 16, 17). Particle deposition is described by a dimensionless parameter α , known as the attachment efficiency. In deep bed filtration theory, the attachment efficiency is controlled only by nanoparticle-collector interactions and is independent of particle concentration because it neglects particle agglomeration during transport in porous media and neglects effects of previously attached particles on deposition, i.e. blocking and ripening (18). Furthermore, it assumes monodisperse particles and irreversible attachment in a primary minimum. These assumptions are not likely to be valid for polymer-modified NZVI transport at high particle concentration (1–10 g/L)

* Corresponding author phone: (412)268-2948; fax: (412)268-7813; e-mail: glowry@cmu.edu.

[†] Department of Civil & Environmental Engineering, Carnegie Mellon University.

[‡] Center for Experimental Study of Subsurface Environmental Processes at Colorado School of Mines.

[§] Department of Chemical Engineering, Carnegie Mellon University.

^{||} Department of Biomedical Engineering, Carnegie Mellon University.

because particles are polydisperse and they tend to agglomerate in porous media due to their magnetic attractive forces (5, 10). Furthermore, polymer modified NZVI is likely to be deposited within a secondary minimum, which is subject to detachment under an external force (i.e., shear force) or from a change of solution chemistry (19–21). Thus, typical deep-bed filtration models may not be appropriate for describing the transport of concentrated NZVI dispersions.

The objective of this research is to determine the fundamental physicochemical processes affecting transport of polyelectrolyte-modified NZVI in porous media at the high particle concentration typically used in groundwater remediation. Specifically, we determine the effect of particle concentration, intrinsic size distribution (prior to agglomeration in porous media), and magnetic attractive forces on the deposition and transport of surface-modified NZVI and propose a new conceptual model for the transport and deposition of surface modified NZVI at high concentration in sand columns. NZVI was modified by physisorption of poly(styrene sulfonate) (PSS), and its colloidal properties were characterized. Particle elution data were collected for PSS-modified NZVI and hematite at particle concentrations ranging from 0.03 to 6 g/L in 5 mM NaCl/5 mM NaHCO₃ (pH = 8). To elucidate the importance of particle size distribution, transport, and deposition of PSS-modified NZVI particles with three different intrinsic particle size distributions were compared. The influence of magnetic attraction on NZVI deposition was assessed by comparing the deposition behavior of PSS-modified NZVI with similarly prepared PSS-modified (nonmagnetic) hematite.

Materials and Methods

PSS-Modified NZVI and Hematite Nanoparticles. Reactive nanoscale iron particles (RNIP), commercially available reactive Fe⁰/Fe₃O₄ core-shell NZVI particles, were obtained from Toda Kogyo, Japan. RNIP consists of a polydisperse suspension of irregularly shaped, sintered particles, with primary particles ranging in size from 5 to 40 nm with a median radius of ~20 nm. Hematite (Fe₂O₃) nanoparticles with a median radius of ~20 nm were obtained from Nanostructured and Amorphous Materials Inc. (Los Alamos, NM). Nanoparticles were sonicated with an ultrasonic probe (550 Sonic Dismembrator, Fisher Scientific) for 30 min to break aggregates formed during their storage. Poly(styrene sulfonate) with a molecular weight of 70 kg/mol (PSS) from Aldrich (St. Louis, MO) was used as a polyelectrolyte modifier for RNIP and hematite. PSS was physisorbed to RNIP in a suspension containing 6 g/L RNIP and 2 g/L PSS as previously described (10). All excess (unadsorbed) PSS was removed from the dispersion prior to use by centrifugation (Sorvall, OTD65B) at 27,500 rpm (or 45,000 g) for 80 min and washing with a solution containing 5 mM NaCl and 5 mM NaHCO₃ (pH 8.0 ± 0.1). The PSS-modified hematite dispersion was prepared in the same manner as PSS-modified RNIP except that the surface modification was done at 10 g/L hematite and 4 g/L PSS for convenience. Stable suspensions of hematite could be formed at a higher concentration because of its lower rate of aggregation compared to RNIP.

Particle Fractionation. To examine the effect of intrinsic particle size distribution on transport, PSS-modified RNIP dispersions with three different intrinsic particle size distributions were prepared by sequential, quiescent sedimentation. The sedimentation times were selected to provide measurably distinct particle size distributions as measured by dynamic light scattering. The unfractionated PSS-modified RNIP dispersion was designated PSS-RNIP-F1. The fractionation procedure was as follows. After 20 min of quiescent sedimentation, 80 vol% of the supernatant was removed and settled for 12 h. Particles remaining in the upper 80 vol% of the supernatant were designated as PSS-RNIP-F3 (~0.8% of

particles by mass), while the settled particles and lower 20 vol% of the supernatant were designated as PSS-RNIP-F2 (~52% by mass of F1). The unfractionated PSS-modified hematite was designated as PSS-Hematite-F1. The upper 80 vol% of the supernatant remaining stable after 12 h was designated as PSS-Hematite-F2. The surface-modified hematite was very stable so only two size fractions were generated for hematite. All sedimentation and transport experiments were conducted using the same stock particle suspensions. Fractions F2 and F3 were concentrated to 1–6 g/L using an ultracentrifuge, removing excess supernatant, and then diluting with a solution containing 5 mM NaCl and 5 mM NaHCO₃ to obtain a 6 g/L stock dispersion.

The intrinsic particle size distributions of the different PSS-modified nanoparticle fractions were determined by dynamic light scattering (DLS) (Malvern Zetasizer, Southborough, MA) at 5 mg/L particle concentration in DI water. Prior to the measurement, the stock solution was diluted to 5 mg/L in DI water and sonicated for 3 min to break agglomerates formed during storage. This permitted measurement of the intrinsic size distribution of primary particles and (unbreakable) sintered aggregates. The CONTIN algorithm was used to convert intensity autocorrelation functions to intensity-weighted particle hydrodynamic diameter distributions, assuming the Stokes–Einstein relationship for spherical particles. The volume- and number-weighted particle size distributions of RNIP were insensitive to the choice of refractive index, i.e. using refractive index values for either Fe⁰ ($n = 2.87 + 3.35i$) or Fe₃O₄ ($n = 2.42$) yielded similar particle size distributions (the difference is <5%).

Fe⁰ Content. RNIP is a Fe⁰/Fe-oxide core/shell particle. Fe⁰ is magnetic so the Fe⁰ content affects RNIP aggregation and sedimentation (5, 10). The Fe⁰ content of RNIP was determined (separately from total iron) by digesting particles with HCl (2M, trace metal grade) in a closed container and measuring H₂ in the headspace as described previously (2, 10). Total iron (Fe⁰ + Fe-oxides) was determined by atomic absorption spectrometry (AA) after acid digestion. The Fe⁰ content (%) and total RNIP concentration were calculated from these measurements. Method details are described in refs 2 and 10 and in the Supporting Information.

Polyelectrolyte Surface Excess Concentration. The adsorbed mass of PSS on nanoparticles was determined by the solution depletion method. The concentration of PSS in the supernatant of both PSS-modified RNIP and hematite was measured by absorbance at 225 nm (extinction coefficient = 0.04 L mg⁻¹ cm⁻¹) using a UV–vis spectrophotometer (Varian, Palo Alto, CA). The adsorbed mass of PSS was determined by the difference between the total added PSS concentration and the unadsorbed PSS concentration measured after ultracentrifugation and was normalized to the particle concentration and its N₂–BET specific surface area of 15 and 22 m²/g for RNIP and hematite, respectively, to obtain the surface excess concentration (mg PSS/m²).

Adsorbed PSS Layer Characterization. The adsorbed PSS layer was characterized using electrophoretic mobility (EPM) measurements and Ohshima's soft particle theory (22) as previously described (10). Details of Ohshima's method can be found in refs 10 and 22 and in the Supporting Information. Briefly, the EPM was measured for 10 mg/L solutions of the washed, PSS-modified RNIP for all three RNIP fractions, PSS-RNIP-F1, -F2, and -F3, and the two hematite fractions, PSS-Hematite-F1 and -F2, at NaCl concentrations ranging from 1 to 61 mM (pH 8.0 ± 0.1). The EPM was measured in triplicate (25 °C) using a Malvern Zetasizer (Southborough, MA). The mean and standard deviation (σ) of the measured EPM (u_e) were calculated. The procedure for extracting the adsorbed polyelectrolyte layer properties from the EPM data involves fitting Ohshima's model to obtain the best fit layer properties including charge density in the adsorbed polyelectrolyte layer

TABLE 1. Physical Properties of Different Fractions of PSS-Modified RNIP and Hematite

particle	fraction	mode	average R_H nm: %		Γ (mg/m ²)	d (nm)	Fe ⁰ (%)	stable fraction with respect to sedimentation (% by mass) ^a
			1 st peak	2 nd peak				
PSS-RNIP	F1	vol.	45:6	328:94	2.1 ± 0.4	63 ± 15	62.6 ± 5.1	3
		no.	26:98	263:2				
	F2	vol.	25:40	367:60	1.5 ± 0.7	75 ± 24	9.6 ± 0.5	4
		no.	15:100	-				
	F3	vol.	24:100	-	1.5 ± 0.7	75 ± 12	4 ± 0.1	50
		no.	16:100	-				
PSS-Hematite	F1	vol.	155:100	-	1.5 ± 0.7	41 ± 2	0	80
		no.	81:100	-				
	F2	vol.	62:100	-	1.5 ± 0.7	46 ± 3	0	90
		no.	38:100	-				

^a Stable fraction is defined as the mass % of particles remaining suspended and measurable by absorption at 508 nm after 7 h of sedimentation. The initial particle concentration for sedimentation was 1000 mg/L in all cases.

(N), softness parameter (λ), and adsorbed layer thickness (d) for the mean u_e , and the mean $u_e \pm \sigma$ as a function of ionic strength using a MATLAB (the Mathworks, Novi, MI) code employing iterative least-squares minimization. The average and standard deviation of the fitting parameters determined for the mean u_e and the mean $u_e \pm \sigma$ was calculated (Supporting Information Table S1). It should be noted that this procedure is not meant to convey the goodness of fit of the data, rather it is used to bound the range of each fitted parameter (10).

Sedimentation. The sedimentation of PSS-RNIP (-F1, -F3, and -F3) and PSS-Hematite (-F1 and -F2) in 10 mM Na⁺ background electrolyte was determined for different initial RNIP concentrations (30 and 1000 mg/L) by monitoring the optical absorbance at 800 nm as a function of time by UV-vis spectrophotometry (Varian, Palo Alto, CA). All measurements were made at 25 °C in duplicate.

Transport Experiments. Transport studies were performed in stainless steel, 25.5 cm long (1.27-cm o.d. and 1.09-cm i.d.) columns with 1/16" end fittings. Columns were packed wet (6) with spherical silica sand as model porous media ($d_{50} = 300 \mu\text{m}$, Agsco Corp., Hasbrouck Heights, NJ). The average porosity of the packed column was determined gravimetrically to be 0.33. The transport studies were conducted as a function of particle concentration (0.03, 0.3, 1, 3, 6 g/L) for different fractions of PSS-RNIP and hematite at 23 ± 2 °C in 10 mM Na⁺ background electrolyte (pH 8) in an upflow configuration and at a pore water velocity of 3.2×10^{-4} m/s maintained by a peristaltic pump.

Column experiments were conducted as follows. At least 10 pore volumes (PV) of 10 mM Na⁺ (5 mM NaHCO₃ and 5 mM NaCl) were flushed through the column to remove background turbidity and provide a uniform collector surface charge. A particle dispersion of the concentration being evaluated in 10 mM Na⁺ was ultrasonicated for 5 min to break all agglomerates formed during storage and sonicated during up-flow injection thereby injecting particles having the initial intrinsic particle size distribution. One PV of particle dispersion was injected, followed by flushing with 10 mM Na⁺ for 3 PVs to achieve complete breakthrough of the mobile fraction of particles. Effluent samples collected in the fraction collector were analyzed by atomic absorption spectrometry (AA) after acid digestion in concentrated HCl (trace metal grade).

Results and Discussion

Intrinsic Particle Size Distributions for Different Particle Fractions. Sequential, quiescent sedimentation separated PSS-modified nanoparticle dispersions into three different intrinsic particle size distributions (Supporting Information Figure S1). The intrinsic particle size distribution for each

fraction included both primary particles and sintered aggregates but in different ratios. The distribution (volume basis) of the unfractionated dispersion (PSS-RNIP-F1) was bimodal with an average R_H centered at 45 nm and another centered at 325 nm (Table 1). While the lower R_H is consistent with the primary particle size, which is 5 to 40 nm, R_H measured for the second peak is larger than the primary RNIP particles, corresponding to sintered aggregates found in the slurry. However, the larger aggregates account for only 2 number % of the population of PSS-modified RNIP (Table 1 and Figure S1c). PSS-RNIP-F2 was also bimodal with the same average R_H values as PSS-RNIP-F1; however, the fraction of primary particles increased relative to the sintered aggregates as the larger aggregates were removed during quiescent sedimentation (Table 1 and Figure S1a). PSS-RNIP-F3 was monomodal with an average R_H of 25 nm. The unfractionated PSS-Hematite-F1 was monomodal with an average R_H of 115 nm (Figure S1b). After 12 h of sedimentation, the distribution of PSS-Hematite-F2 became monomodal with an average R_H of 62 nm, confirming that larger aggregates of PSS-modified hematite were removed during quiescent sedimentation.

Adsorbed Polymer Layer Characterization, Fe⁰ Content, and Aggregation. The physical properties of different fractions of PSS-modified RNIP and hematite are given in Table 1 and Table S1 in the Supporting Information. The maximum surface excess concentration, Γ_{max} , of PSS-modified RNIP was 2.1 ± 0.4 mg/m², in good agreement with previous reports (10). Γ_{max} of PSS-modified hematite was 1.5 ± 0.7 mg/m². The measured layer thicknesses (d) for the different size fractions of RNIP were similar, indicating that particle size in the range studied here does not significantly impact the conformation of the adsorbed layer. The adsorbed mass and layer thicknesses measured for hematite was slightly less than that measured for RNIP. This difference is attributed to the intrinsic difference between the surfaces of hematite nanoparticles and RNIP which leads to different interactions with PSS and thus different adsorbed conformations. However, the differences are small, and the adsorbed PSS layer properties that control electrosteric repulsions for each modified nanoparticle are expected to be similar for each particle type and size fraction.

Unfractionated PSS-RNIP-F1 (Fe⁰ = 63%) had a significantly higher Fe⁰ content than PSS-RNIP-F2 (10%) and -F3 (4%) (Table 1). This is consistent with expectation because the oxidation of the Fe⁰ core to iron oxide (predominantly magnetite) is a surface mediated reaction so particles with the highest surface-to-volume ratio (i.e., smallest particles such as PSS-RNIP-F3) are expected to be the most oxidized. This difference in Fe⁰ content can have a significant impact

TABLE 2. Magnitude of 2nd Minimum Well and Distance from the Surface Where It Occurs for Particle-Particle Interaction of Each Fraction of PSS70K-RNIP and Hematite

particle	fraction	peak no.	average R _H (nm) by vol.	M _s (kA/m)	2 nd minimum well (k _B T)	distance from the surface where 2 nd minimum occurs (nm)	N _{flow} (10 ⁻⁴)
PSS70K-RNIP	F1	1	328	1105	-3528.2	125	0.17
		2	45	1105	-955.4	110	0.01
	F2	1	367	495	-808.0	123	0.94
		2	25	495	-6.3	145	0.66
PSS70K-Hematite	F3	1	24	400	-3.3	151	1.20
	F1	1	155	0	-0.6	82	150.04
	F2	1	62	0	-	-	-

TABLE 3. C/C₀ and Corresponding α_{exp} for PSS-RNIP and PSS-Hematite Fractions at Different Initial Particle Concentrations

particle	fraction	particle concentration			
		30 mg/L		1–6 g/L	
		C/C ₀	Log α _{exp}	C/C ₀	Log α _{exp}
PSS-RNIP	F1	0.92	-1.95	0.60–0.63	-1.14 to -1.18
	F2	0.90	-2.27	0.77–0.79	-1.87 to -1.92
	F3	0.90	-2.61	0.9–0.97	-2.60 to -3.13
PSS-Hematite	F1	0.89	-1.93	0.9–0.97	-1.96 to -2.50
	F2	0.90	-2.29	0.93–0.95	-2.43 to -2.58

on agglomeration, deposition, and transport as discussed subsequently.

The agglomeration and sedimentation of PSS-modified RNIP increased with increasing Fe⁰ content and particle size (Table 1). The adsorbed layer properties for all particles were similar, so the extent and reversibility of aggregation were mainly controlled by the magnitude of the magnetic attraction between particles. Magnetic attraction is proportional to Fe⁰ content and scales with particle radius to the sixth power (5, 10). The effect of Fe⁰ on agglomeration and sedimentation is evident from the greater agglomeration (sedimentation) of PSS-RNIP-F1 compared to PSS-RNIP-F2, which have similar particle size distributions but have substantially different Fe⁰ content. The effect of particle size on agglomeration cannot be ignored given the r⁶ dependence. Agglomeration (sedimentation) of PSS-RNIP-F2 is greater than PSS-RNIP-F3 even though both have similar Fe⁰ content. The difference is attributed to the substantially different particle size distribution.

This is semiquantitatively explained using extended DLVO theory that includes both magnetic attraction and electrosteric repulsions, in addition to conventional DLVO forces as described in ref 10. A representative force profile for PSS-RNIP is provided in the Supporting Information (Figure S3). Even with the large electrosteric energy barrier between PSS-modified RNIP, agglomeration in a secondary minimum is predicted at a distance ~2d between two RNIP particles (10) due to the strong magnetic attractive force between particles. The depth of the secondary minimum well for each particle type and the distance where it occurs are summarized in Table 2. PSS-RNIP-F1 and-F2 having the largest sintered aggregates and highest Fe⁰ content, and therefore largest magnetic attraction, are least resistant to agglomeration and sedimentation (Table 1). Further, agglomeration should be less reversible for PSS-RNIP-F1 and-F2 due to the deeper secondary minimum well (-7 to > -3000 k_BT) compared to PSS-RNIP-F3 which has only small primary particles, less Fe⁰, and a shallower energy well (~3 k_BT) (Table 2). Here, k_B is the Boltzmann constant (1.381 × 10⁻²³ m² kg s⁻² K⁻¹) and T is the absolute temperature (298 K in this study). Hematite nanoparticles are nonmagnetic so the electrosteric energy barrier provided by adsorbed PSS can overcome van der Waals

attraction between hematite nanoparticles. A very shallow secondary minimum energy well is predicted, and 80 to 90% of the PSS modified hematite-F1 and F2 remain stable against aggregation (Table 1, Table 2, and Figure S3b in the Supporting Information). The qualitative trends for the effect of particle size and Fe⁰ content on agglomeration discussed here are indicative of agglomeration behavior for a dynamic environment with fluid shear such as during transport in porous media as discussed in detail later.

Particle Transport at Low Particle Concentration, 30 mg/L. This low particle concentration satisfies the assumptions of clean bed filtration models, so C/C₀ at the plateau (Table 3) of the breakthrough curves (Figure S4a in the Supporting Information) was used to calculate the experimental attachment efficiency, α_{exp} using eq 1 (23)

$$\alpha_{\text{exp}} = -\ln\left(\frac{C}{C_0}\right) \frac{4a_c}{3(1-\epsilon)\eta_0 L} \quad (1)$$

Here, L is the bed depth, a_c is the average radius of a collector (150 μm silica sand in this study), and ε is the porosity of the clean bed media which is 0.33. η₀ is calculated using Tufenkji and Elimelech's correlation (24). The experimental attachment efficiency α_{exp} values for all polyelectrolyte modified particles were similar (i.e., log α_{exp} values from approximately -2 to -2.6), indicating that at low particle concentration the deposition characteristics of all polymer-modified nanoparticles were similar, regardless of particle size distribution or magnetic properties. This experimental result suggest that under these conditions neither particle agglomeration in porous media nor media ripening effects were significant and that the transport of PSS-modified nanoparticles at low particle concentration was controlled only by particle-collector interaction as suggested by filtration theory. The negligible effect of particle size on deposition in clean bed filtration under unfavorable deposition conditions is consistent with theory (25, 26).

Particle Transport at High Particle Concentration, 1–6 g/L. The deposition behaviors of three size fractions of PSS-modified RNIP at concentrations of 1, 3, and 6 g/L are different (Figure 1), implying that in addition to particle-collector interactions, agglomeration in porous media plays a substantial role. The maximum normalized concentrations of

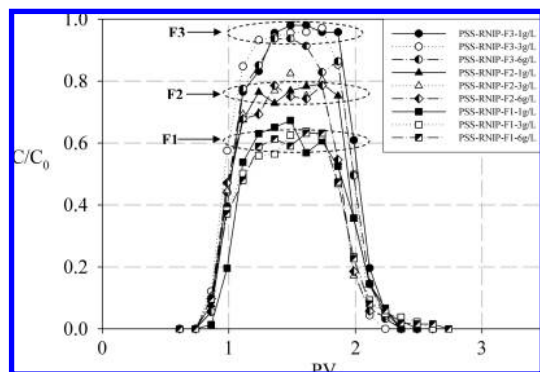


FIGURE 1. Normalized breakthrough curves of different PSS-RNIP fractions for particle concentrations between 1 and 6 g/L through a water-saturated sand ($d_p = 300 \mu\text{m}$) 5 mM NaCl/5 mM NaHCO_3 at a pore water velocity of 3.2×10^{-4} m/s.

breakthrough curves and calculated α_{exp} values are given in Table 3. The deposition of PSS-RNIP-F1 and -F2, having the largest preformed clusters and highest Fe^0 content, was greater than deposition of PSS-RNIP-F3, with only small primary particles and low Fe^0 content, and greater than deposition of nonmagnetic hematite particles (Figure S4b in the Supporting Information). For a given particle size fraction, however, the particle concentration over the range 1 to 6 g/L did not affect deposition and transport (Figure 1) indicating that the particle concentration itself had almost no effect on the deposition efficiency over this concentration range. Presumably, at higher particle concentrations, the agglomeration reaches steady state, i.e. the formation of the stable sized agglomerates, quickly (27) (see also the Supporting Information). However, the size of the agglomerates formed should be similar regardless of particle concentration because the size is solely controlled by force balance (28) as discussed in the last section.

Despite being modified with similar adsorbed PSS layers, at high particle concentration (1–6 g/L), fractions with high agglomeration tendencies in porous media (large sized preformed clusters and high Fe^0 content) showed less transport through the columns. This observation is different from the transport at low concentration where only particle-collector interaction controls the deposition as described in the previous section. This finding can be explained by particle agglomeration during transport in porous media and subsequent deposition as described next.

Particle Agglomeration and Subsequent Deposition in Porous Media. Classic deep bed filtration models technically cannot be used to model the observed deposition of PSS-RNIP at high particle concentration because these models ignore agglomeration of particles expected during transport in porous media. Such models would use the size of primary particles, aggregates, or agglomerates entering the column (or aquifer) to predict deposition and may yield inaccurate predictions. An alternative conceptual model of particle/cluster agglomeration in porous media and subsequent deposition (Figure 2) is more appropriate for explaining the deposition behavior of PSS-RNIP at high particle concentration. This conceptual model assumes that stable agglomerates form quickly in porous media (see the Supporting Information) under a secondary minimum between particle–particle or particle-cluster interactions. The agglomerate size is a result of the balance between van der Waals and magnetic attractions between PSS-RNIP particles, electrosteric repulsive forces from the adsorbed PSS, and the induced fluid shear in the pore spaces. Therefore, the agglomerates formed in PSS-RNIP-F1 should be larger than PSS-RNIP-F2 and much larger than PSS-RNIP-F3, because the particle/cluster sizes and Fe^0 content which promote agglomeration of different

PSS-RNIP fractions follow the order of $F1 > F2 > F3$. The agglomerates then transport and deposit onto a collector (e.g., a sand grain). Larger agglomerate sizes yield higher attachment efficiency because the drag force due to the fluid flow (which promotes detachment) is less than the adhesive force which promotes particle attachment when the size of the retained particles/agglomerates increases (20) (see the Supporting Information). This is consistent with the observed deposition of PSS-RNIP-F1, -F2, and -F3 where PSS-RNIP with larger particles and higher Fe^0 content (-F1 and -F2) formed larger stable agglomerates due to stronger magnetic attraction between particles.

Agglomeration Tendency. Experimental results and the conceptual model of agglomeration and subsequent deposition suggest that, at high particle concentration, the agglomeration tendency in porous media of PSS-RNIP-F1 is higher than PSS-RNIP-F2 which is much larger than PSS-RNIP-F3, and this should be responsible for the limited transport of -F1 and -F2 in comparison to -F3. In this section, we apply the concept of the aggregate formation in a batch system with fluid shear to semiquantitatively support the hypothesis of agglomeration in porous media in this study.

In a system with a constant shear rate such as a flow field in porous media (19), the particles entering the column (Figure S1) are continually agglomerating and disagglomerating, ultimately reaching a steady-state agglomerate size (27, 28). The size of stable PSS-RNIP agglomerated is influenced by the shear force and the van der Waals and magnetic attractions between particles, which is a function of Fe^0 content and particle size distribution. Higashitani and Iimura (28) determined that the average number of particles in stable aggregates is inversely proportional to a dimensionless parameter, N_{flow} , which is the ratio of the shear force to the net interparticle attractive force. Considering only van der Waals attraction, N_{flow} can be calculated using eq 2 (28)

$$N_{\text{flow}} = \frac{6\pi\mu a\delta^2\gamma_s}{H} \quad (2)$$

where H is the Hamaker constant, δ is the minimum distance between two adjacent particles in the agglomerate, and γ_s is the shear rate which is calculated assuming that a constricted tube model represents the void space between collectors in the porous media (Figure S6 in the Supporting Information). The PSS-RNIP agglomerates form under a secondary minimum (Table 2) resulting from electrosteric repulsions as well as van der Waals and magnetic attraction. Therefore, for our particles eq 2 is modified as follows: δ for our study is the distance where the secondary minimum occurs (Table 2). H is substituted with an equivalent Hamaker constant, H_{equiv} , defined as the effective Hamaker constant that yields the appropriate depth of the secondary minimum well (Table 2) accounting for the contribution of all interparticle forces. N_{flow} for PSS-RNIP-F3 is two times larger than N_{flow} for PSS-RNIP-F2 and one to 2 orders of magnitude larger than N_{flow} for PSS-RNIP-F1 (Table 2). However, N_{flow} for PSS-RNIP-F3 is 2 orders of magnitudes smaller than N_{flow} for PSS-hematite-F1. This suggests that the stable agglomerates formed in polydisperse PSS-RNIP dispersions with a greater fraction of large sintered aggregates and higher Fe^0 contents (F1 and F2) contain more particles and are larger than agglomerates formed in PSS-RNIP-F3 dispersions that contain only small primary particles and low Fe^0 content. Stable agglomerates in hematite dispersions that lack magnetic attractions are predicted to be significantly smaller than any of the PSS-RNIP. Further, the larger agglomerates of PSS-RNIP-F1 and -F2 deposit more irreversibly than individual particles or small agglomerates of PSS-RNIP-F3 during transport at moderate and high particle concentration where agglomeration becomes important. This is consistent with

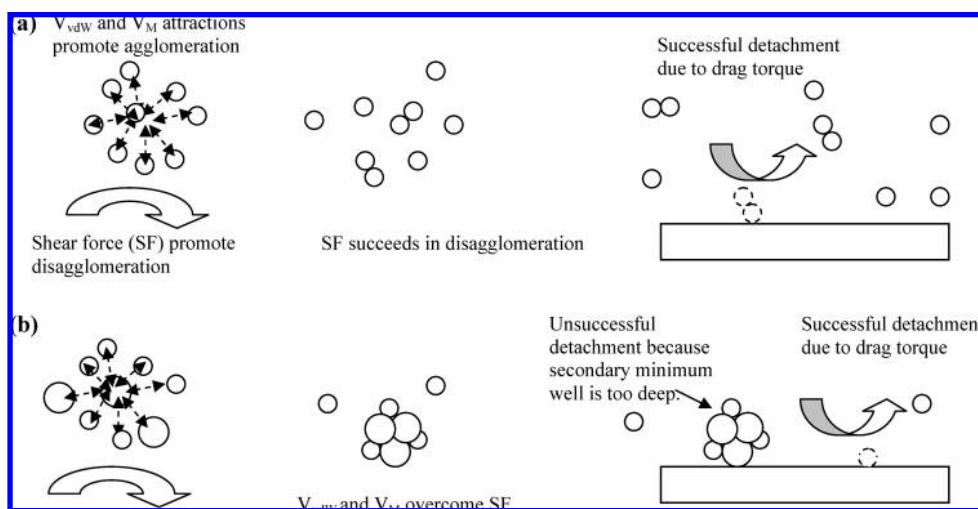


FIGURE 2. Conceptual model of agglomeration of polydisperse PSS-modified RNIP followed by deposition of clusters under a secondary minimum. This model considers the balance of shear force (which is a function of fluid velocity) and total attraction energy between particles and/or aggregates (which is a function of ionic strength, van der Waals attraction, magnetic attraction, and electrostatic repulsions) on agglomeration and disagglomeration, together with the balance between secondary minimum between clusters and collectors and drag torque on attachment and detachment: (a) small less polydisperse particles with low Fe^0 content and (b) large more polydisperse particles with higher Fe^0 content.

the observed deposition behavior of the different PSS-RNIP size distributions discussed previously.

Implications for Field Application of NZVI. This study is the first attempt to systematically evaluate the importance of intrinsic particle size distribution, magnetic properties, and particle concentration of polyelectrolyte surface modified NZVI on their transport in porous media. Both particle size distribution and Fe^0 content of NZVI, which are normally overlooked, are important properties affecting NZVI mobility in porous media. Deep bed filtration models appear to be valid for modeling the deposition of PSS-RNIP at low concentration (30 mg/L). This is important for assessing the risk of unwanted migration away from the point of application where low particle concentrations are expected at the fringe of the injection site, but deep bed filtration models fail at high particle concentration (1–6 g/L) because the particles agglomerate during transport. Deep bed filtration theory will have to be modified to account for agglomeration to be useful for predicting NZVI transport and emplacement of NZVI in porous media.

Smaller particles with low Fe^0 content travel farther than those with high Fe^0 content. However, Fe^0 is essential for dechlorination or heavy metal reduction and immobilization. Methods that assess the radius of influence (ROI) or extent of the treatment zone created by NZVI injection should therefore include assessment of Fe^0 content because measurements such as total iron or visual methods (e.g., cores) may overestimate the extent of migration of the reactive NZVI (29). The results also suggest that synthetic methods (such as the use of dopants or multiple magnetic domain particles) to maximize Fe^0 content while minimizing magnetic attractive forces between particles should afford high NZVI reactivity and enhance NZVI transport in porous media. Another alternative to enhance the mobility of NZVI in porous media is to create a more extended or denser adsorbed polyelectrolyte layer on NZVI which can decrease the extent of particle aggregation but may also decrease reactivity (30). Supporting the Fe^0 onto larger particles such as hydrophilic carbon or onto clay particles (13, 14) or silica matrix (8) may also be a viable alternative to minimizing the aggregation of these particles and enhancing their mobility.

Acknowledgments

This research was funded in part by the U.S. EPA (R833326), the NSF (BES-068646 and EF-0830093), the Department of Defense through the Strategic Environmental Research and Development Program (W912HQ-06-C-0038), and the Royal Thai Government through a fellowship to Tanapon Phenrat.

Supporting Information Available

Fe^0 content determination via acid digestion; Ohshima's soft particle analysis to estimate adsorbed polyelectrolyte layer properties on NZVI; equations for the constricted tube model to estimate apparent shear rate acting on aggregates in porous media and shear experienced by a retained particle at the pore wall; characteristics of the adsorbed polyelectrolyte layers estimated by Ohshima's soft particle analysis; secondary minimum wells for particle-collector interactions as a function of the sizes of PSS-RNIP particles/agglomerates; particle size distributions for each particle fraction; sedimentation curves; extended DLVO predictions for particle-particle and particle-collector interactions; breakthrough curves; diameter of pore (d_p) as a function of distance from the center of a collector (z) according to the constricted tube model; and calculated T_{applied} and T_{adhesive} for different sizes of PSS70K modified RNIP. This material is available free of charge via the Internet at <http://pubs.acs.org>.

Literature Cited

- Tratnyek, P. G.; Johnson, R. L. Nanotechnologies for environmental cleanup. *Nano Today* **2006**, *1* (2), 44–48.
- Liu, Y.; Phenrat, T.; Lowry, G. V. Effect of TCE concentration and dissolved groundwater solutes on NZVI-promoted TCE dechlorination and H_2 evolution. *Environ. Sci. Technol.* **2007**, *41* (22), 7881–7887.
- Li, X.-q.; Zhang, W.-x. Sequestration of Metal Cations with Zerovalent Iron Nanoparticles—A Study with High Resolution X-ray Photoelectron Spectroscopy (HR-XPS). *J. Phys. Chem. C* **2007**, *111* (19), 6939–6946.
- Henn, K. W.; Waddill, D. W. Utilization of nanoscale zero-valent iron for source remediation - A case study. *Rem. J.* **2006**, *16*, 57–77.
- Phenrat, T.; Saleh, N.; Sirk, K.; Tilton, R. D.; Lowry, G. V. Aggregation and sedimentation of aqueous nanoscale zerovalent iron dispersions. *Environ. Sci. Technol.* **2007**, *41* (1), 284–290.

- (6) Saleh, N.; Sirk, K.; Liu, Y.; Phenrat, T.; Dufour, B.; Matyjaszewski, K.; Tilton, R. D.; Lowry, G. V. Surface modifications enhance nanoiron transport and NAPL targeting in saturated porous media. *Environ. Eng. Sci.* **2007**, *24* (1), 45–57.
- (7) Kanel, S. R.; Goswami, R. R.; Clement, T. P.; Barnett, M. O.; Zhao, D. Two Dimensional Transport Characteristics of Surface Stabilized Zero-valent Iron Nanoparticles in Porous Media. *Environ. Sci. Technol.* **2008**, *42* (3), 896–900.
- (8) Zhan, J.; Zheng, T.; Piringer, G.; Day, C.; McPherson, G. L.; Lu, Y.; Papadopoulos, K.; John, V. T. Transport Characteristics of Nanoscale Functional Zerovalent Iron/Silica Composites for in Situ Remediation of Trichloroethylene. *Environ. Sci. Technol.* **2008**, *42* (23), 8871–8876.
- (9) Phenrat, T.; Lowry, G. V. Physicochemistry of polyelectrolyte coatings that increase stability, mobility, and contaminant specificity of reactive nanoparticles used for groundwater remediation. In *Nanotechnology Applications for Clean Water*; Savage, N., Mamadou, D., Duncan, J. S., Street, A., Sustich, R. C., Eds.; William Andrew: Norwich, NY, 2009; pp 249–267.
- (10) Phenrat, T.; Saleh, N.; Sirk, K.; Kim, H.-J.; Tilton, R. D.; Lowry, G. V. Stabilization of aqueous nanoscale zerovalent iron dispersions by anionic polyelectrolytes: adsorbed anionic polyelectrolyte layer properties and their effect on aggregation and sedimentation. *J. Nanopart. Res.* **2008**, *10*, 795–814.
- (11) Saleh, N.; Kim, H.-J.; Matyjaszewski, K.; Tilton, R. D.; Lowry, G. V. Ionic Strength and Composition affect the mobility of surface-modified NZVI in water-saturated sand columns. *Environ. Sci. Technol.* **2008**, *42* (9), 3349–3355.
- (12) He, F.; Zhao, D.; Liu, J.; Roberts, C. B. Stabilization of Fe-Pd Nanoparticles with Sodium Carboxymethyl Cellulose for Enhanced Transport and Dechlorination of Trichloroethylene in Soil and Groundwater. *Ind. Eng. Chem. Res.* **2007**, *46* (1), 29–34.
- (13) Schrick, B.; Hydutsky, B. W.; Blough, J. L.; Mallouk, T. E. Delivery vehicles for zerovalent metal nanoparticles in soil and groundwater. *Chem. Mater.* **2004**, *16* (11), 2187–2193.
- (14) Hydutsky, B. W.; Mack, E. J.; Beckerman, B. B.; Skluzacek, J. M.; Mallouk, T. E. Optimization of Nano- and Microiron Transport through Sand Columns Using Polyelectrolyte Mixtures. *Environ. Sci. Technol.* **2007**, *41* (18), 6418–6424.
- (15) Saleh, N.; Phenrat, T.; Sirk, K.; Dufour, B.; Ok, J.; Sarbu, T.; Matyjaszewski, K.; Tilton, R. D.; Lowry, G. V. Adsorbed triblock copolymers deliver reactive iron nanoparticles to the oil/water interface. *Nano Lett.* **2005**, *5* (12), 2489–2494.
- (16) Lecoanet, H. F.; Bottero, J.-Y.; Wiesner, M. R. Laboratory assessment of the mobility of nanomaterials in porous media. *Environ. Sci. Technol.* **2004**, *38* (19), 5164–5169.
- (17) Wang, Y.; Li, Y.; Fortner, J. D.; Hughes, J. B.; Abriola, L. M.; Pennell, K. D. Transport and retention of nanoscale C_{60} aggregates in water-saturated porous media. *Environ. Sci. Technol.* **2008**, *42* (10), 3588–3594.
- (18) Elimelech, M.; Gregory, J.; Jia, X.; Williams, R. *Particle Deposition and Aggregation: Measurement, Modeling, and Simulation*; Butterworth-Heinemann: Boston, 1995.
- (19) Bergendahl, J.; Grasso, D. Prediction of colloid detachment in a model porous media: hydrodynamics. *Chem. Eng. Sci.* **2000**, *55*, 1523–1532.
- (20) Torkzaban, S.; Bradford, S. A.; Walker, S. L. Resolving the coupled effects of hydrodynamics and DLVO forces on colloid attachment in porous media. *Langmuir* **2007**, *23*, 9652–9660.
- (21) Franchi, A.; O'Melia, C. R. Effects of Natural Organic Matter and Solution Chemistry on the Deposition and Reentrainment of Colloids in Porous Media. *Environ. Sci. Technol.* **2003**, *37* (6), 1122–1129.
- (22) Ohshima, H. Electrophoresis of soft particles. *Adv. Colloid Interface Sci.* **1995**, *62*, 189–235.
- (23) Saleh, N.; Kim, H.-J.; Phenrat, T.; Matyjaszewski, K.; Tilton, R. D.; Lowry, G. V. Ionic Strength and Composition Affect the Mobility of Surface-Modified Fe⁰ Nanoparticles in Water-Saturated Sand Columns. *Environ. Sci. Technol.* **2008**, *42* (9), 3349–3355.
- (24) Tufenkji, N.; Elimelech, M. Correlation equation for predicting single-collector efficiency in physicochemical filtration in saturated porous media. *Environ. Sci. Technol.* **2004**, *38*, 529–536.
- (25) Elimelech, M.; O'Melia, C. R. Effect of particle size on collision efficiency in the deposition of Brownian particles with electrostatic energy barriers. *Langmuir* **1990**, *6* (6), 1153–1163.
- (26) Elimelech, M. Predicting collision efficiencies of colloidal particles in porous media. *Water Res.* **1992**, *26* (1), 1–8.
- (27) Spicer, P. T.; Pratsinis, S. E.; Trennepohl, M. D.; Meesters, G. H. M. Coagulation and fragmentation: the variation of shear rate and the time lag for attainment of steady state. *Ind. Eng. Chem. Res.* **1996**, *35*, 3074–3080.
- (28) Higashitani, K.; Iimura, K. Two-dimensional simulation of the breakup process of aggregates in shear and elongational flows. *J. Colloid Interface Sci.* **1998**, *204*, 320–327.
- (29) Bergendahl, J.; Grasso, D. Prediction of colloid detachment in a model porous media: hydrodynamics. *Chem. Eng. Sci.* **2000**, *55*, 1523–1532.
- (30) Phenrat, T.; Liu, Y.; Tilton, R. D.; Lowry, G. V. Adsorbed polyelectrolyte coatings decrease Fe⁰ nanoparticle reactivity with TCE in water: conceptual model and mechanisms. *Environ. Sci. Technol.* **2009**, *43* (5), 1507–1514.

ES900171V